J Mater Sci: Mater Med (2007) 18:71–78
DOI 10.1007/s10856-006-0664-y

Contact damage in an yttria stabilized zirconia: Implications for biomedical applications

J. Zhou · J. Mah · P. Shrotriya · C. Mercer · W. O. Soboyejo

Received: 20 October 2005 / Accepted: 28 February 2006

Abstract This paper presents the results of a combined experimental and computational study of contact damage in a 3 mole% yttria partially stabilized zirconia (3-YSZ) that is relevant to hip implants and dental restorations. Contact-induced loading in real applications is idealized using Hertzian contact model to explain plasticity phenomena and failure mechanisms observed under monotonic and cyclic loading. Under monotonic loading, the elastic moduli increase with increasing loading levels. Under cyclic loading, the ceramic specimens fail with progressive cone cracking. X-ray analyses reveal that stress-induced phase transformation (from tetragonal to monoclinic phases) occurs under cyclic contact loading above the critical load levels (∼8.5 kN). Furthermore, when the cyclic loading level (5.0 kN) is less than a critical load levels (7.5 kN) that is required to induce surface cone cracks, significant plastic damage is observed in the subsurface zone underneath the contact area. These suggest that the cyclic contact loading induce both plastic damage and tetragonal-to-monoclinic phase transformation in the 3-YSZ, leading to significant degradation in long-term strength. The implications of the results are discussed for the design of zirconia femoral heads in total hip replacements and zirconia crowns in dental restoration.

J. Zhou (✉) · J. Mah · W. O. Soboyejo
Princeton Institute for Science and Technology of Materials, and Department of Mechanical and Aerospace Engineering, Princeton University, Princeton, NJ 08544
e-mail: soboyejo@princeton.edu

P. Shrotriya
Department of Mechanical Engineering, Iowa State University, Ames, IA 50011

C. Mercer
Materials Department, University of California, Santa Barbara, CA 93106

Introduction

Zirconia-based ceramics and alumina-based ceramics have been increasingly used as implant biomaterials [1–6]. They have been used to make crowns in dental restorations for decades [3–5]. Due to their excellent resistance to wear and friction, they have also been used in hip implants recently (Fig. 1(a)) [7, 8]. In such biomedicine applications, one of the most serious concerns with ceramic implants is the possible fatigue failure. Almost 20% of the ceramic crowns fail within 5 years of use [9]. Under cyclic contact loading, these bioceramics may fail with surface cone cracks or subsurface radial cracks (Fig. 1(b)) [1]. Thus, the orthopedic applications of ceramic hips/knees, and dental restoration implants must be designed against possible fatigue failure [10–14].

A 3 mole% yittria-stabilized zirconia (3-YSZ) is one of the most frequently used ceramics for these applications [15]. It displays a quasi-plastic yielding behavior. Plasticity in ceramics occurs almost exclusively due to fault sliding resulting from subsurface shear stresses or phase transformation, in which tetragonal phase is transformed into monoclinic phase. The phase transformation induced inhomogeneous stress field make the failure mechanisms even more complicated. In light of the recent troubles surrounding zirconia femoral heads in hip implants [16, 17] and the failure in zirconia crowns, the objective of this study is to investigate the contact-induced deformation behavior and failure mechanisms of 3-YSZ under monotonic and cyclic Hertzian contact loading. To simplify the analysis, all the tests are carried out on a monolithic 3-YSZ layer. We find that the zirconia strength is much stronger under monotonic loading than under cyclic loading. Under monotonic loading, the ceramics simply fails due to surface cone crack growth. However, both plastic damage accumulation and phase transformation were observed under cyclic loading. Finite element

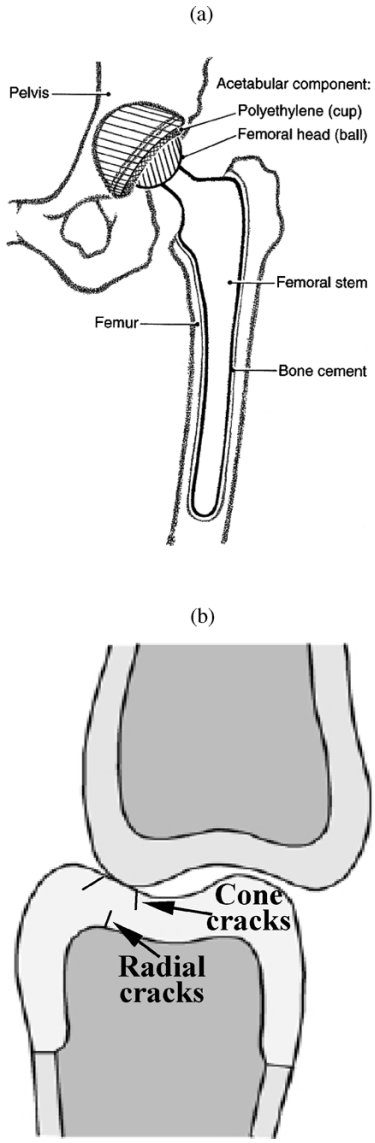

Fig. 1 Schematics of (a) total hip implant structure and (b) Surface cone cracks and subsurface radial cracks induced by Hertzian contact loading

simulations were also used to study the stress fields associated with Hertzian contact loading. The implications of the results are discussed for biomedical applications of 3-YSZ in contact loading.

Materials and methods

3 mole% yttria stabilized zirconia (3-YSZ) material used in this study was obtained from Incerco (Rushville, IN). The material was produced using hot-isostatic pressing (HIPing) of zirconia powders to produce medical grade zirconia compacts. To examine the microstructure of the zirconia compacts, they were diamond polished to a mirror finish, and followed by thermal etching in air. This was achieved by slowly ramping the furnace temperature up to 1400°C, holding at 1400°C for one hour, and slowly cooling to room temperature to avoid thermal shock effects. Scanning electron microscopy (SEM) images of the thermally etched microstructure are presented in Fig. 2. This shows a bimodal grain microstructure, consisting of small grains ($\sim$1 μm in diameter) and larger grains ($\sim$5 μm in diameter). The material also contained some porosity, as shown in Fig. 2(a). No compositional varieties in the two types of grains are observed in a backscatter electron image (Fig. 2(b)).

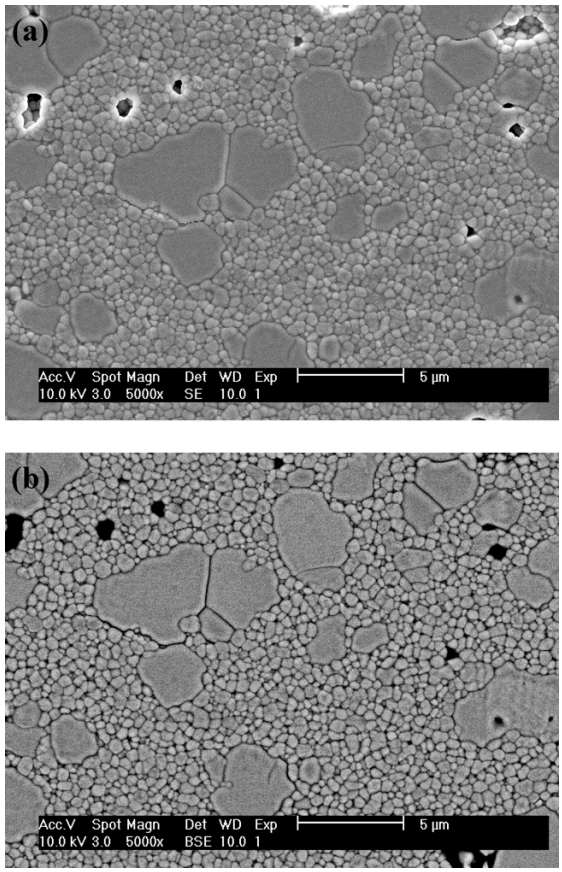

Fig. 2 Bimodal grain structure of 3-YSZ ceramics: (a) secondary electron SEM image and (b) back-scattered electron image

Zirconia specimens (10 mm $\times$ 10 mm $\times$ 10 mm) were tested in an Instron 8872 servo-hydraulic desktop testing machine (Instron, Canton, MA). A tungsten indenter with a diameter of 20 mm was used. A capacitance gage was used to record displacement of the zirconia induced by the tungsten indenter. The testing set up is shown schematically in Fig. 3(a). The experimental set up is the same for both monotonic and cyclic testing.

Samples for cyclic testing were prepared in three different ways. The first group of cyclic tests was conducted on samples prepared identically to those for the monotonic test. The data gathered from this first group of cyclic tests was

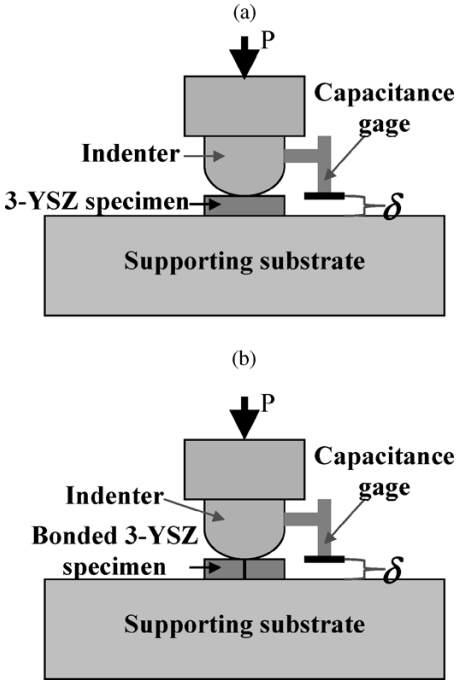

Fig. 3 Schematic test-setup: (a) monotonic and cyclic testing; (b) 3-YSZ specimen is divided into two pieces to facilitate subsurface damage investigation after testing

used to obtain data on displacement versus cyclic number (N). The second group of cyclic tests was used to investigate the cone crack evolution with increasing cyclic number. The tests were stopped after loading for 1, 10, 10^2, 10^3, 10^4 and 10^5 cycles for surface examination using SEM. The third group testing was designed to provide insights into the micro-mechanisms of subsurface deformation underneath the contact area. Instead of one solid sample piece, two sample pieces of identical height were held flush against each other in a small vice. The samples were then subjected to Hertzian contact loading, as shown schematically in Fig. 3(b). After testing, the two sample pieces were separated, and the subsurface deformation was studied using SEM. This revealed the subsurface deformation patterns that were induced as a result of stress field that were present beneath the indentor.

Cyclic testing was carried out at a stress ratio of 0.1 and at a cyclic frequency of 10 Hz. Sinusoidal loading profiles were applied, since no evidence of contact-induced surface cone cracks was observed at loading below 7.5 kN, and because the 10 kN specimens failed after only ~100 cycles, most of the zirconia compacts were loaded to a peak load of 8.5 kN for durations up to 10^5 cycles. In an effort to avoid the effects of the surface cone cracks, a low loading level of 5.0 kN was used to study subsurface damage accumulation in the subsurface regions right underneath the contact area.

Contact mechanics and finite element modeling

Hertzian contact mechanics

In this study, the contact loads were applied to flat zirconia ceramic samples using a semispherical tungsten indenter. This is shown schematically in Fig. 3(a). The initial contact-induced deformation and stress fields can be modeled using Hertzian contact mechanics [18, 19]. This is shown schematically in Fig. 2(a). The mechanical responses of the zirconia are dependent on the material properties of the contact surfaces and geometry of the system. The radius of the circular contact area is given by [18]:

$$a = \sqrt[3]{\frac{3PR}{4E'}} \tag{1}$$

where P is the applied contact load and R is the radius of the spherical tungsten indentor. The reduced modulus, E', is given by [18]

$$\frac{1}{E'} = \frac{1-\nu_1^2}{E_1} + \frac{1-\nu_2^2}{E_2} \tag{2}$$

where E_1 and E_2 are the moduli of the tungsten carbine indenter and zirconia, respectively, ν_1 and ν_2 are the Poisson's radios of tungsten carbide and zirconia, respectively. The elastic properties of relevant materials are summarized in Table 1 [15]. The displacement is defined as the mutual approach of distant points in the two solids. It is given by [18]:

$$\delta = \sqrt[3]{\frac{9P^2}{16RE'^2}} \tag{3}$$

Outside the contact area, the maximum pressure induced by the indenter is given by [18]:

$$\sigma_{\max} = \sqrt[3]{\frac{6PE'^2}{\pi^3 R^2}} \tag{4}$$

To obtain valid Hertzian contact testing, it is important to ensure that the edges of the sample piece do not overlap the Hertzian stress fields. Thus, the sample size has to be of adequate thickness and surface area. Typical requirements include [10]: $5a \leq {}^1\!/_2\, d$, $5a \leq t$, $5a \leq R$, where d is the minimum value of the specimen length or width, and t is the

Table 1 Elastic parameters of Tungsten and Zirconia [15]

Materials	Tungsten	Zirconia
Poisson's Ratio, ν	0.28	0.28
Young's modulus E, (GPa)	400	205

specimen thickness. In this study, the diameter of the tungsten carbide ball was 20 mm, and the reduced modulus was ∼147 GPa. When the applied contact load was less than 19 kN, the radius of the contact area was roughly estimated from Eq. (1) to be less than 0.1 mm. Hence, the sample dimensions were selected to be greater than 10 mm × 10 mm × 10 mm.

Finite element simulations

Finite element simulations of the Hertzian contact-induced deformation were carried out using the ABAQUS software package (Hibbit, Karlsson and Sorenson, Inc. Pawtucket, RI). Axissymetric idealizations of the ball/zirconia configurations (Fig. 3(a)) were used in the simulations, along with 6 node quadratic triangular elements. The tungsten ball was assumed to be rigid, while zirconia samples were deformable. Hertzian indentation loads, corresponding to actual values applied in the experiments, were applied in incremental stages using one of the sub-routines within ABAQUS. The corresponding stress distributions were calculated using the constitutive equations for elastic deformation.

Results and discussions

Compressive deformation behavior under monotonic contact loading

The first sample was tested to estimate the ceramic strength under Hertzian contact loading. The sample broke at a load level of ∼19 kN, due to cone crack propagation across the sample thickness. Corresponding to this critical load, the strength of zirconia ceramics was estimated to be ∼9 GPa using Eq. (4). Subsequent monotonic tests were carried out to study changes in ceramic stiffness with increasing maximum load levels. Each sample was loaded for one cycle (load and unload) at a constant loading/unloading rate of 5 N/sec. This was done for maximum applied loads of 3 kN, 8 kN, 12 kN, 15 kN, and 17 kN. Typical load/unloading curves (of load versus displacement) are shown in Fig. 4(a), for the specimens that were subjected to a load of 8 kN. Based on Hertzian contact theory [18], the relationship between load and displacement (Eq. (3)) may be rewritten as:

$$P = \sqrt{\frac{16}{9} R E'^2 \delta^3} \tag{5}$$

Taking logarithms of both sides of Eq. (5), we may reduce Eq. (5) to the following linear relationship:

$$\log P = \log (\mathrm{C}) + 3/2 \log \delta \tag{6}$$

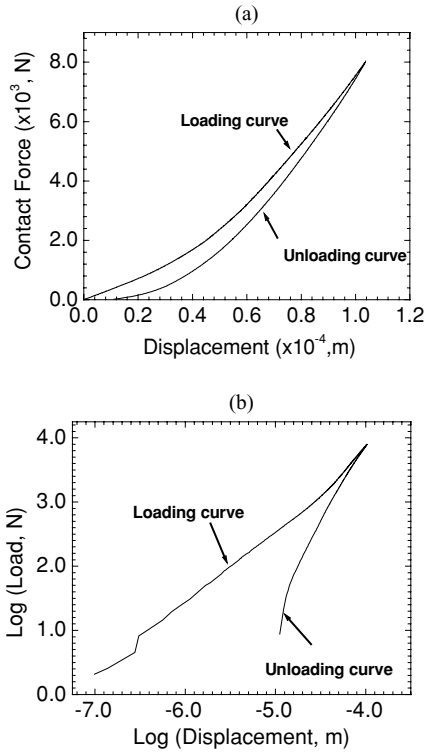

Fig. 4 Load/unloading-displacement curves corresponding to monotonic loading up to 8.0 kN: (a) The loading/unloading curves; and (b) the same curves in (a) plotted on log-log scale

where $C = \sqrt{\frac{16}{9} R E'^2}$, is determined by the contacted materials properties and indenter radius. Assuming that no property change occurs in the tungsten indentor, any change of C can be attributed to the changes in Young's Moduli and Poissson's ratio of the zirconia. Since the Poisson's ratio is unlikely to change significantly for both materials, the change in elastic modulus of zirconia was inferred from the plots of log of the measured load versus log of the displacement. Figure 4(b) is the log-log plot of data shown in Fig. 4(a). Once a linear curve is fitted from the unloading curve, the intercept of the load axis, b, corresponds to Log C, i.e. $b = \mathrm{Log}\ C$. The elastic modulus of zirconia ceramic is then estimated from the following equation:

$$E_1 = \frac{1 - \nu_1^2}{\frac{1}{\frac{10^b \times 3}{4\sqrt{R}}} - \frac{1-\nu_2^2}{E_2}} \tag{7}$$

A plot of Young's modulus versus maximum load level is presented in Fig. 5. This shows that the effective Young's modulus of the zirconia increases with increasing maximum load level. This could be attributed to material densification due to increasingly applied loads. Lou and Stevens measured the Young's muduli of 3 mole% YSZ with different porosity, and found that the modulus increased from 53 GPa to 219 GPa

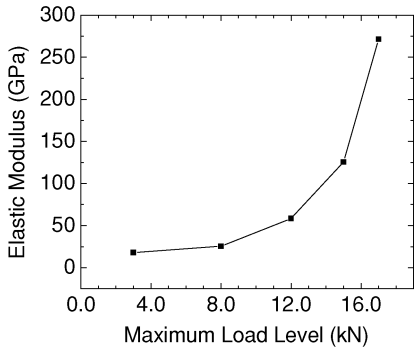

Fig. 5 A plot of Young's modulus versus maximum load level

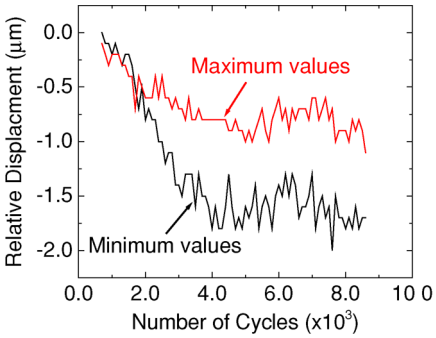

Fig. 6 A plot of peak-to-trough relative displacement as functions of the number of cycles

as the ceramic porosity decreased from 0.38 to 0 [20]. Our measured modulus values are consistent with the reported data, indicating the existence of porosity is one major factor that causes changes in the modulus under monotonic loading.

Failure mechanisms under cyclic contact loading

Cyclic loading of single specimens of zirconia was carried out under Hertzian contact loading at a load range of 0.85 kN to 8.5 kN (both in compression) and a frequency of 10 Hz. Figure 6 shows the peak-to-trough displacement response of the zirconia sample during the test. The test was stopped after 8600 load cycles, after a displacement plateau was reached. It should be noted that the overall contact induced displacement in zirconia is in the micrometer order. The displacement in the initial stage is less than 0.5 μm. This is less than the measurement resolution of the capacitance gage (1.0 μm), leading to the inaccuracy in displacement measurement. These explain why the trough relative displacement is higher than the peak relative displacement within first two thousand cycles in Fig. 6.

The important point in Fig. 6 is the gradual increase in magnitude of the resultant displacements of the zirconia sample. Both the maximum and minimum displacements increased with increasing number of fatigue cycles, resulting in increased penetration of the samples by the indenter. This leads ultimately to irreversible subsurface and surface damage, for load levels above a critical threshold value.

The evolution of contact-induced damage observed on the surfaces of the 3-YSZ compacts is shown in Fig. 7. Evidence of contact-induced damage is present even after the very first fatigue cycle (Fig. 7(a)). This is in the form of circumferential cone cracks and permanent indents remains on the surface upon removal of the applied load. Subsequent cyclic contact results in the progressive formation of cone cracks and increasing crack opening (Figs. 7(b)–(f)). The spacing between the cone cracks is almost constant Fig. 7(f), and

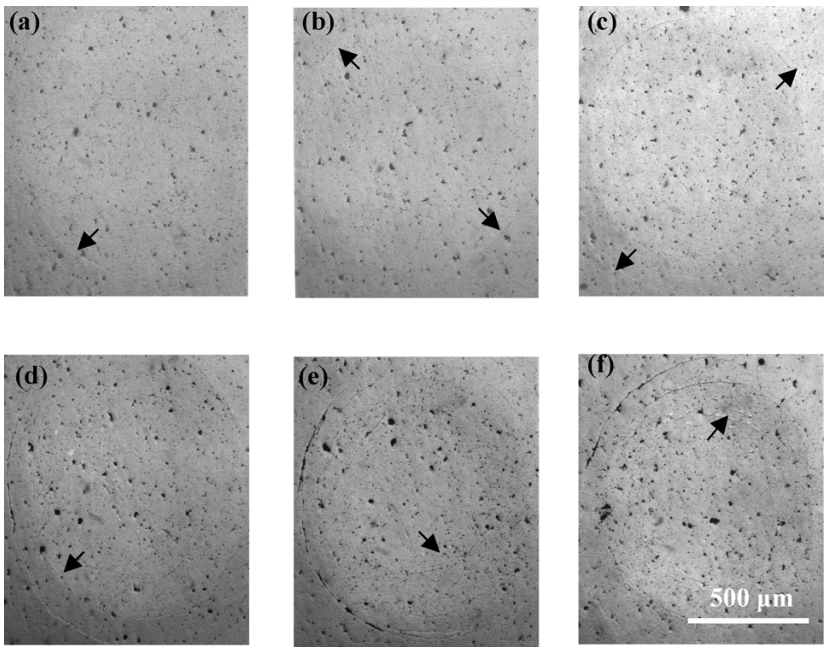

Fig. 7 Evolution of contact damage in zirconia due to fatigue loading at a peak load of 8.5 KN: (a) $N = 10^0$ cycles, (b) $N = 10^1$ cycles, (c) $N = 10^2$ cycles, (d) $N = 10^3$ cycles, (e) $N = 10^4$ cycles and (f) $N = 10^5$ cycles

the residual indentations become more pronounced, as the number of fatigue cycle increases. This suggests a mechanism of quasi-plasticity that involves stress-induced phase transformations [21–26] and circumferential/ring cracking phenomena (Figs. 7(a)–(f)).

The principal stress distributions associated with the Hertzian indentation of the zirconia compacts is presented in Fig. 8. This shows clearly that the cone cracks are induced largely as a result of the circular symmetry of the principal stress distributions. Since the sizes of the high stress regions will increase with incremental cyclic deformation, the observation of more cone cracks and increasing crack opening is consistent with a progressive cyclic deformation mechanism that involves incremental plasticity and cracking. However, further work is needed to develop a more complete understanding of the relative contributions of stress-induced phase transformations and cracking phenomena to the overall levels of quasi-plasticity.

The most telling sign of permanent damage during cyclic loading tests is the formation of dimples underneath the contact area. Figures 9(a) and (b) show the subsurface damage of the divided zirconia sample piece after 100,000 cycles of 0.5 kN to 5.0 kN sinusoidal loading. This damaged zone is the lighter section in Fig. 9(a), and it consists of pore and cone cracks that are induced by tensile stresses at the edge of the quasi-plastic zone (Fig. 9(b)). It should be noted that Fig. 9(b) is amplified image of the selected area B in Fig. 9(a). These radiate down from the surface, at roughly a 45 degree angle. The SEM picture in Fig. 9(a) provides evidence of the considerable damage accumulated in the test sample. However, without looking below the surface of the sample, such behavior can go un-noticed. It is also important to note that the observed fatigue deformation and cracking modes occur at stress levels are considerably below those required for the failure of PSZ under monotonic loading.

In an effort to establish whether the cyclic loading cause stress-induced phase transformations, X-ray diffraction analysis was carried out on specimens that were subjected to cyclic Hertzian contact loading after 10^5 cycles. X-ray diffraction analysis procedure has been described in a previous study [27]. Two loading ranges were used: 0.65–6.5 kN and 0.85–8.5 kN. Undeformed samples were also characterized as a control. No observable phase transformation was detected in the specimens that were loaded to 6.5 kN. However, in the specimens loaded to 8.5 kN, the volume fraction of monoclinic phase increased significantly from ~14.7% to 24.5%. The X-ray diffraction analysis results are listed in Table 2. This suggests that significant phase transformation is induced by cyclic contact loading. Moreover, a critical load level is required to initiate phase transformation at room temperature. This critical load level is between 6.5 and 8.5 kN for current experimental set up used in this study.

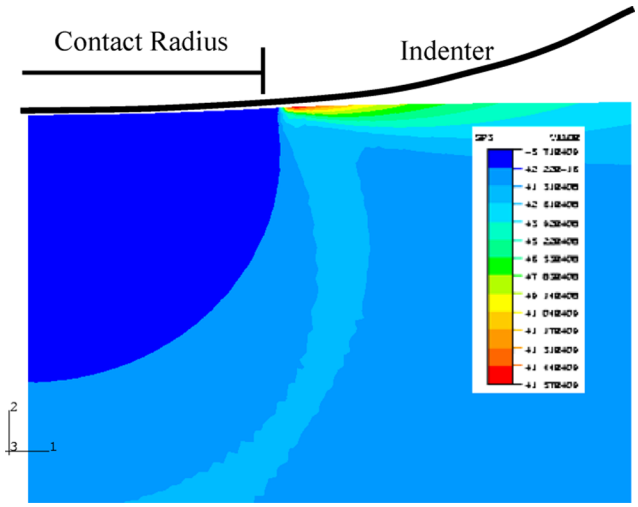

Fig. 8 Principal stress distributions in zirconia subjected to a contact load of 8.5 kN

Implications

The current work shows that incremental deformation can occur by circumferential cone cracking (Figs. 8(a)–(f)) and stress-induced phase transformations. The progressive nature of the cone cracking also suggests that significant fatigue damage accumulation does occur in the load range (8.5–0.85 kN) that was examined in this study. However, the observed cone cracks would not be acceptable in clinical practice. A threshold-based approach is, therefore, recommended. In the case of the biomedical grade 3 mole% yttria stabilized zirconia material examined in this study, the threshold appears to be ~ 6.5 kN at a stress ratio of 0.1, since there is no surface cone crack developed when the applied maximum load is less than 6.5 kN. Also, there is no phase transformation occurs at this load level. Further work is clearly needed to establish the fatigue thresholds as functions of grain size and yttria composition.

Finally, it is important to note that this work has not considered the possible effects of biomedical environments on fatigue processes. Since such environments could lead to stress corrosion cracking and other types of environmentally-assisted processes. It is recognized that contact-induced fa-

Table 2 X-ray diffraction analysis of phase transformation induced by contact indentation

Load range	Sample	Monoclinic phase (volume %)
0.65 kN–6.5 kN	Undeformed	18.1
	Indented	18.0
0.85 kN–8.5 kN	Undeformed	14.7
	Indented	24.5

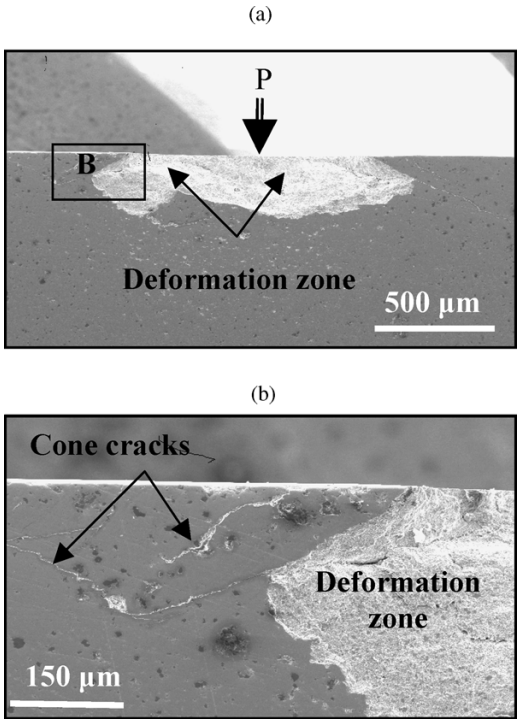

Fig. 9 Damage of a zirconia sample piece after 100,000 cycles (Sample tested at a load range between 0.5 kN to 5.0 k): (a) overview of subsurface deformation zone; and (b) cone cracks and pores are observed at a higher magnification

tigue, like all fatigue, is clearly environmentally-assisted [15]. Further work is clearly needed to develop mechanism-based models for the prediction of environmentally-assisted contact fatigue in biomedical environments.

Concluding remarks

This paper presents the results of a study of contact-induced deformation and cracking in 3-YSZ that is used in biomedical applications. Salient conclusions arising from this study are summarized below:

1. Under monotonic loading, the Young's moduli of 3-YSZ ceramics increase with increasing load levels. This is attributed to the material densification when increasing load levels are applied.
2. Cyclic contact damage above a Hertzian contact load of 6.5 kN results in the initiation and evolution of surface cone cracks. The initiation of the cone cracks is associated with the maximum principle stresses. Contact-induced phase transformation from tetragonal to monoclinic phases was observed under cyclic loading between 0.85–8.5 kN.
3. 3-YSZ ceramics used in dental crowns and hip implants may fail due to the sub-critical fatigue damage at the load levels that are significantly lower than those required for damage 3-YSZ under monotonic loading. A fatigue threshold-based design approach is recommended. The threshold appears to be ∼6.5 kN at a stress ratio of 0.1.

Acknowledgment This research is supported by the Natinal Institute of Health (NYU/PHS No. F5262-07) and The National Science Foundation (NSF DMR-0231418). The authors are grateful to NIH Program Manager (Dr. Eleni Kouslevari) and NSF Program Manager (Dr. Carmen Huber) for their encouragement and support.

References

1. W. O. SOBOYEJO, C. MERCER, S. A. ALLAMEH, B. NEMETSKI, N. MARCANTONIO and J. L. RICCI, *Key Eng. Mater.* **198–199** (2001) 203.
2. R. R. SEGHI and J. A. SORENSEN, *Int. J. Prosthodontics* **8** (1995) 239.
3. I. M. PETERSON, A. PAJARES, B. R. LAWN, V. P. THOMPSON and E. D. REKOW, *J. Dent. Res.* **77** (1998) 589.
4. D. K. KIM, Y. G. JUNG, I. M. PETERSON and B. R. LAWN, *Acta Mater.* **47** (1999) 4711.
5. R. J. KELLY, *Annual Rev. Mater. Sci.* **27** (1997) 443.
6. R. R. SEGHI, I. DENRY and S. F. ROSENSTIEL, *J. Prosth. Dent.* **74** (1995) 145.
7. L. HENCH and J. W. WILSON, "An Introduction to Bioceramics," (World Scientific, Singapore, 1993).
8. P. CHRISTEL, A. MEUNIER, J. M. DORLOT, J. WITVOLET, L. SEDEL and P. BORITIN, *Annal. N. Y. Acad. Sci.* **523** (1988) 234.
9. L. PRUITT, J. KOO, C. M. RIMNAC, S. SURESH and J. M. WRIGHT, *J. Bone Joint Sur.* **13** (1995) 143.
10. F. BURNY, D. MUSTER, M. DONKERWOKKE and Magerat-Burny, *MRS Bulletin* **25** (2000) 15.
11. B. RATNER, A. S. HOFFMAN, F. J. SCHOEN and J. E. LEMONS, "Biomaterials Science: An Introduction to Materials in Medicine," (Academic Press, New York, NY, 1996).
12. C. M. RIMNAC, T. M. WRIGHT, D. L. BARTEL and A. H. BURSTEIN, Failure Analysis of a Total Hip Femoral Component. In Case Histories involving Fatigue and Fracture Mechanics, ASTM STP 918, American Society for Testing and Materials, West Conshohocken, PA, (1986), p. 377.
13. L. PRUITT, J. KOO, C. M. RIMNAC, S. SURESH and J. M. WRIGHT, *J. Bone Joint Sur.* **13** (1995) 143.
14. K. A. MALAMENT and SOCRANSKY, *J. Pros. Dentist.* **81** (1999) 23.
15. W. O. SOBOYEJO, "Mechanical Properties of Engineered Materials," (Marcel Dekker, New York, 2003).
16. Food and Drug Administration. "Recall of Zirconia Ceramic Femoral Heads for Hip Implants," (September 13, 2001).
17. Associated Press. "Artificial Hips Are Being Recalled," (Washington Post September 14, 2001).
18. K. L. JOHNSON, "Contact Mechanics," (Cambridge University Press, London, UK, 1985).
19. SATAPORN, WUTTIPHAN, "Contact Damage and Fracture of Ceramic Layer Structures," (1997).
20. J. LUO and R. STEVENS, *Porosity-Dependence of Elastic Moduli and Hardness of 3Y-TZP Ceramics, Ceramics International* **25** (1999) 281.
21. S. TIMOSHENKO and S. WOINOWSKY-KRIEGER, "Theory of Plates and Shells," (McGraw Hill Book Company, New York, NY, 1959).
22. A. G. EVANS and R. M. CANON, *Acta Metallurgica* **34** (1986) 761.

23. W. O. SOBOYEJO, D. BROOKS, L. C. CHEN and R. J. LEDERICH, *J. Amer. Cer. Soc.* **78** (1995) 1481.
24. D. B. MARSHALL, M. C. SHAW, R. H. DAUSKARDT, R. O. RITCHIE, M. J. READEY and A. H. HEUER, *J. Amer. Cer. Soc.* **78** (1990) 2659.
25. A. H. HEUR, N. CLAUSSEN, W. M. KRIVEN and M. RUHLE, *J. Amer. Cer. Soc.* **85** (1982) 642.
26. F. F. LANGE, *J. Mater. Sci.* **17** (1982) 225.
27. M. LI, H. SCHAFFER and W. O. SOBOYEJO, *J. Mater. Sci.* **35** (2000) 1339.